

The cusp effect in $\eta' \rightarrow \eta\pi\pi$ decays

Bastian Kubis, Sebastian P. Schneider

Helmholtz-Institut für Strahlen- und Kernphysik (Theorie) and Bethe Center for Theoretical Physics, Universität Bonn, D-53115 Bonn, Germany

Abstract. Strong final-state interactions create a pronounced cusp in $\eta' \rightarrow \eta\pi^0\pi^0$ decays. We adapt and generalize the non-relativistic effective field theory framework developed for the extraction of $\pi\pi$ scattering lengths from $K \rightarrow 3\pi$ decays to this case. The cusp effect is predicted to have an effect of more than 8% on the decay spectrum below the $\pi^+\pi^-$ threshold.

PACS. 11.30.Rd Chiral symmetries – 13.25.Jx Decays of other mesons – 13.75.Lb Meson-meson interactions

1 Introduction

In the last few years, the investigation of the cusp effect in the decay $K^+ \rightarrow \pi^0\pi^0\pi^+$ has become one of the most precise methods to extract S-wave pion-pion scattering lengths from experiment [1–6]. Very loosely speaking, the cusp in the invariant mass spectrum of the $\pi^0\pi^0$ pair is generated by the decay $K^+ \rightarrow \pi^+\pi^+\pi^-$ followed by charge-exchange rescattering $\pi^+\pi^- \rightarrow \pi^0\pi^0$, plus the fact that the pion mass difference shifts the $\pi^+\pi^-$ threshold into the physical region (see also [7]). What makes this channel particularly apt for an investigation of the cusp, apart from the enormous statistics collected by the NA48/2 collaboration [3], is the significantly larger branching fraction of $K^+ \rightarrow \pi^+\pi^+\pi^-$ compared to $K^+ \rightarrow \pi^0\pi^0\pi^+$, such that the perturbation of the decay spectrum of the latter is very sizeable. This is in marked contrast to two other decays that have been studied subsequently and that display, in principle, cusp structures generated by the same mechanism: $K_L \rightarrow 3\pi^0$ [2, 4, 8, 9], and $\eta \rightarrow 3\pi^0$ [8, 10–14]. In both of these, the weaker coupling to the charged-pion final state diminishes the cusp to a mere 1–2% effect on the decay spectrum.

In this respect, $\eta' \rightarrow \eta\pi^0\pi^0$ decays offer a more promising candidate for an alternative channel to study the cusp.¹ Indeed, in the isospin limit $\text{BR}(\eta' \rightarrow \eta\pi^+\pi^-) = 2\text{BR}(\eta' \rightarrow \eta\pi^0\pi^0)$, so one expects a sizeable effect on the $\pi^0\pi^0$ decay spectrum. In this article, we adapt the non-relativistic effective field theory (NREFT) formalism developed in [5, 6, 8] to these channels. Compared to $K \rightarrow 3\pi$ and $\eta \rightarrow 3\pi$ decays, there is a different “secondary” final-state rescattering channel $\pi\eta$ to take into account. In addition, the formalism has to be slightly amended for particles in the final state whose mass difference ($M_\eta - M_\pi$ in this case) is not small. This study is very timely with

regards to the upcoming high-statistics η' experiments at ELSA [16], MAMI-C [17, 18], WASA-at-COSY [19, 20], KLOE-at-DAΦNE [21, 22], or BES-III [23], which are expected to increase the data basis on η' decays by orders of magnitude.

The outline of this article is as follows. In Sect. 2, we present the generalized non-relativistic effective field theory framework for $\eta' \rightarrow \eta\pi\pi$ decays, define the necessary Lagrangians and perform the matching to Dalitz plot as well as $\pi\pi$ and $\pi\eta$ threshold parameters. Furthermore, we comment on the effects of inelastic channels. In Sect. 3, we present the result for the decay amplitudes up to two loops, including radiative corrections. This section comprises the central result of this study and can be used in forthcoming experimental analyses of these decays. We turn around the argument and *predict* the size and specific shape of the cusp in Sect. 4. Our findings are summarized in Sect. 5.

2 NREFT for $\eta' \rightarrow \eta\pi\pi$

We consider the neutral and charged decay modes

$$\begin{aligned}\eta'(P_{\eta'}) &\rightarrow \pi^0(p_1)\pi^0(p_2)\eta(p_3), \\ \eta'(P_{\eta'}) &\rightarrow \pi^+(p_1)\pi^-(p_2)\eta(p_3).\end{aligned}\tag{1}$$

The charged channel only serves as an “auxilliary mode” for the cusp analysis. The kinematical variables are defined in the usual way $s_i = (P_{\eta'} - p_i)^2$, $s_1 + s_2 + s_3 = M_{\eta'}^2 + M_1^2 + M_2^2 + M_3^2$, with $p_i^2 = M_i^2$, $i = 1, 2, 3$. We will use the notation $M_{\pi^\pm} = M_\pi$ throughout.

We shall proceed along the lines of [5] to develop the modified non-relativistic Lagrangian framework for our calculation. It is set up in such a way that the results are manifestly covariant, with the correct analytic structure of the decay amplitude fully reproduced in the low-energy region. A consistent power counting scheme can be

¹ The cusp in this channel is briefly discussed in the framework of unitarized chiral perturbation theory in [15].

constructed in a very similar manner to the one in [5, 8]: we introduce the formal non-relativistic parameter ϵ and count the pion and η 3-momenta (in the η' rest frame) as $\mathcal{O}(\epsilon)$, the kinetic energies $T_i = p_i^0 - M_i$ as $\mathcal{O}(\epsilon^2)$, and the masses of the particles involved as $\mathcal{O}(1)$. Let us remark, however, that as opposed to the case of $\pi\pi$ -scattering, where the mass difference between the two scattering particles amounts to a small contribution in isospin breaking at maximum, for $\pi\eta$ -scattering we count $M_\eta - M_\pi = \mathcal{O}(1)$. We will thus provide a Lagrangian framework that reproduces the low-energy expansion in a standard manner.

The loop expansion using this non-relativistic Lagrangian framework produces a correlated expansion in ϵ and $\pi\pi$ as well as $\pi\eta$ threshold parameters, which we denote summarily by $a_{\pi\pi}$ and $a_{\pi\eta}$, respectively, or by a in case we refer generically to both. Each two-particle-rescattering increases the order of the loop contribution by $a\epsilon$ [5].

2.1 Non-relativistic Lagrangians

The full non-relativistic Lagrangian can be split up into separate parts describing the $\eta' \rightarrow \eta\pi\pi$ tree amplitude and the $\pi\pi$ - and $\pi\eta$ -final state interactions:

$$\mathcal{L} = \mathcal{L}_{\eta'} + \mathcal{L}_{\pi\pi} + \mathcal{L}_{\pi\eta} . \quad (2)$$

The $\eta' \rightarrow \eta\pi\pi$ Lagrangian up to $\mathcal{O}(\epsilon^4)$ is given by

$$\begin{aligned} \mathcal{L}_{\eta'} = & 2\eta'^{\dagger} W_{\eta'} (i\partial_t - W_{\eta'}) \eta' \\ & + \frac{1}{2} \sum_{i=0}^2 G_i \left(\eta'^{\dagger} (W_\eta - M_\eta)^i \eta \Phi_0 \Phi_0 + h.c. \right) \\ & + G_3 \left(\eta'^{\dagger} \eta (W_0^2 \Phi_0 \Phi_0 - W_0 \Phi_0 W_0 \Phi_0) + h.c. \right) \\ & + \sum_{i=0}^2 H_i \left(\eta'^{\dagger} (W_\eta - M_\eta)^i \eta \Phi_+ \Phi_- + h.c. \right) \\ & + H_3 \left(\eta'^{\dagger} \eta (W_\pm^2 \Phi_+ \Phi_- + \Phi_+ W_\pm^2 \Phi_- \right. \\ & \quad \left. - 2W_\pm \Phi_+ W_\pm \Phi_-) + h.c. \right) + \dots , \end{aligned} \quad (3)$$

where Φ , η , η' denote non-relativistic pion, η , and η' field operators, $W_a = \sqrt{M_a^2 - \Delta}$, where Δ is the Laplacian, and G_i , H_i are the low-energy couplings in the neutral and charged channel, respectively. The ellipsis stands for higher orders in the ϵ expansion.

We start with $\pi\pi$ final state interactions and consider the three channels in (i) ($\pi^a \pi^b \rightarrow \pi^c \pi^d$): (00) $(00; 00)$, (x) $(+-; 00)$, $(+-)$ $(+-; +-)$. For the following discussion we introduce the notation

$$\begin{aligned} (\Phi_n)_\mu &= (\mathcal{P}_n)_\mu \Phi_n , & (\Phi_n)_{\mu\nu} &= (\mathcal{P}_n)_\mu (\mathcal{P}_n)_\nu \Phi_n , \\ (\Phi_n^\dagger)_\mu &= (\mathcal{P}_n^\dagger)_\mu \Phi_n^\dagger , & (\Phi_n^\dagger)_{\mu\nu} &= (\mathcal{P}_n^\dagger)_\mu (\mathcal{P}_n^\dagger)_\nu \Phi_n^\dagger , \\ (\mathcal{P}_n)_\mu &= (W_n, -i\nabla) , & (\mathcal{P}_n^\dagger)_\mu &= (W_n, +i\nabla) , \end{aligned} \quad (4)$$

for $n = a, b, c, d$. Analogous definitions hold for derivatives on the η field, with $\Phi \rightarrow \eta$ and $\mathcal{P}_n \rightarrow \mathcal{P}_\eta$. The $\pi\pi$ -final

state Lagrangian can be written as [8]

$$\mathcal{L}_{\pi\pi} = 2 \sum_{k=0,\pm} \Phi_k^\dagger (i\partial_t - W_k) \Phi_k + \sum_i \mathcal{L}_i , \quad (5)$$

where the first part is the free pion propagator and

$$\begin{aligned} \mathcal{L}_i = & x_i C_i \left(\Phi_c^\dagger \Phi_d^\dagger \Phi_a \Phi_b + h.c. \right) \\ & + x_i D_i \left\{ (\Phi_c^\dagger)_\mu (\Phi_d^\dagger)^\mu \Phi_a \Phi_b + \Phi_c^\dagger \Phi_d^\dagger (\Phi_a)_\mu (\Phi_b)^\mu \right. \\ & \quad \left. - h_i \Phi_c^\dagger \Phi_d^\dagger \Phi_a \Phi_b + h.c. \right\} \\ & + x_i F_i \left\{ (\Phi_c^\dagger)_{\mu\nu} (\Phi_d^\dagger)^{\mu\nu} \Phi_a \Phi_b + \Phi_c^\dagger \Phi_d^\dagger (\Phi_a)_{\mu\nu} (\Phi_b)^{\mu\nu} \right. \\ & \quad + 2(\Phi_c^\dagger)_\mu (\Phi_d^\dagger)^\mu (\Phi_a)_\nu (\Phi_b)^\nu + h_i^2 \Phi_c^\dagger \Phi_d^\dagger \Phi_a \Phi_b \\ & \quad - 2h_i \left((\Phi_c^\dagger)_\mu (\Phi_d^\dagger)^\mu \Phi_a \Phi_b + \Phi_c^\dagger \Phi_d^\dagger (\Phi_a)_\mu (\Phi_b)^\mu \right) \\ & \quad \left. + h.c. \right\} + \dots , \end{aligned} \quad (6)$$

with $x_{00} = 1/4$, $x_x = x_{+-} = 1$ and $h_i = s_i^t - \frac{1}{2}(M_a^2 + M_b^2 + M_c^2 + M_d^2)$, where s_i^t is the physical threshold of the i th channel, explicitly $h_{00} = 2M_{\pi^0}^2$, $h_x = 3M_\pi^2 - M_{\pi^0}^2$, $h_{+-} = 2M_\pi^2$. We have omitted P-wave contributions (in the $(+-)$ channel) as they do not contribute in $\eta' \rightarrow \eta\pi\pi$ as long as conservation of C-parity is assumed. The ellipsis denotes the omission of higher-order terms in the ϵ expansion.

In the case of $\pi\eta$ scattering, we consider the channels (i) ($\eta\pi^a \rightarrow \eta\pi^a$): $(\eta 0)$ $(\eta 0; \eta 0)$, $(\eta +)$ $(\eta +; \eta +)$ [the $\eta\pi^- \rightarrow \eta\pi^-$ amplitude is identical to $\eta\pi^+ \rightarrow \eta\pi^+$ by charge conjugation]. For the $\pi\eta$ Lagrangian we find

$$\mathcal{L}_{\pi\eta} = 2\eta^\dagger W_\eta (i\partial_t - W_\eta) \eta + \sum_i \mathcal{L}_i , \quad (7)$$

where the first term is again the free particle propagator. Before giving the explicit form of the interaction piece, we define a differential operator

$$\hat{s}^{-1} \doteq \left[M_\eta^2 + M_a^2 + (\mathcal{P}_\eta^\dagger)_\mu (\mathcal{P}_a^\dagger)^\mu + (\mathcal{P}_\eta)_\mu (\mathcal{P}_a)^\mu \right]^{-1} . \quad (8)$$

This operator has to be understood as follows: expand about the respective thresholds $s_{\eta\pi^0}^t = (M_\eta + M_{\pi^0})^2$ and $s_{\eta\pi}^t = (M_\eta + M_\pi)^2$,

$$\begin{aligned} \hat{s}^{-1} \eta^\dagger \Phi_a^\dagger \eta \Phi_a + h.c. = & \frac{1}{(M_\eta + M_a)^2} \left(\eta^\dagger \Phi_a^\dagger \eta \Phi_a + h.c. \right) \\ & + \frac{1}{(M_\eta + M_a)^4} \left((\eta^\dagger)_\mu (\Phi_a^\dagger)^\mu \eta \Phi_a + \eta^\dagger \Phi_a^\dagger (\eta)_\mu (\Phi_a)^\mu \right. \\ & \quad \left. - s_{\eta a}^t \eta^\dagger \Phi_a^\dagger \eta \Phi_a + h.c. \right) + \dots , \end{aligned}$$

then apply the Feynman rules of the theory in momentum space and resum the result. Note that the differential operator \hat{s}^{-1} does not violate analyticity and unitarity of the S-Matrix in the low-energy region, since it is obeyed term by term.

We can now display the interaction piece

$$\begin{aligned} \mathcal{L}_i = & C_i (\Phi_a^\dagger \eta^\dagger \Phi_a \eta + h.c.) \\ & + D_i \left\{ (\eta^\dagger)_\mu (\Phi_a^\dagger)^\mu \eta \Phi_a + \eta^\dagger \Phi_a^\dagger (\eta)_\mu (\Phi_a)^\mu - h_i \eta^\dagger \Phi_a^\dagger \eta \Phi_a \right. \\ & \quad \left. + \Delta_{\eta a}^2 \hat{s}^{-1} \eta^\dagger \Phi_a^\dagger \eta \Phi_a + h.c. \right\} \\ & + \frac{E_i}{2} \left\{ \left((\eta^\dagger)_\mu (\Phi_a^\dagger)_\mu - (\eta^\dagger)_\mu \Phi_a^\dagger \right) \left((\eta)_\mu \Phi_a + \eta (\Phi_a)^\mu \right) \right. \\ & \quad \left. - \Delta_{\eta a}^2 \hat{s}^{-1} \eta^\dagger \Phi_a^\dagger \eta \Phi_a + h.c. \right\} + \dots, \end{aligned} \quad (9)$$

with $h_{\eta 0} = M_\eta^2 + M_{\pi^0}^2$, $h_{\eta+} = M_\eta^2 + M_\pi^2$, and $\Delta_{\eta a} = M_\eta^2 - M_a^2$. The ellipsis again stands for higher-order terms in ϵ . We do not consider six-particle couplings, since their contribution to the amplitude is negligible (see Sect. 2.3).

2.2 Matching

We obtain the couplings of $\mathcal{L}_{\eta'}$ by matching to the standard Dalitz plot distribution

$$|\mathcal{M}(x, y)|^2 = |\mathcal{N}|^2 (1 + ay + by^2 + dx^2 + \dots), \quad (10)$$

where \mathcal{N} is a normalization constant, and

$$\begin{aligned} x &= \frac{\sqrt{3}(s_1 - s_2)}{2M_{\eta'} Q_{\eta'}} = \frac{\sqrt{3}(p_2^0 - p_1^0)}{Q_{\eta'}}, \\ y &= \frac{(M_\eta + 2M_{\pi^0})[(M_{\eta'} - M_\eta)^2 - s_3]}{2M_{\eta'} M_{\pi^0} Q_{\eta'}} - 1 \\ &= \frac{M_\eta + 2M_{\pi^0}}{M_{\pi^0} Q_{\eta'}} (p_3^0 - M_\eta) - 1, \\ Q_{\eta'} &= M_{\eta'} - M_\eta - 2M_{\pi^0}, \end{aligned} \quad (11)$$

and we have omitted a C-violating term $\propto x$. The particle energies p_i^0 in the η' rest frame are related to the invariants s_i according to

$$p_i^0 = \frac{M_{\eta'}^2 + M_i^2 - s_i}{2M_{\eta'}}. \quad (12)$$

For the charged channel we have to replace $M_{\pi^0} \rightarrow M_\pi$ in (11). Equation (10) is reproduced, up to higher orders in x, y , by the following polynomial amplitude

$$\mathcal{M}(x, y) = \mathcal{N} \left\{ 1 + \frac{a}{2}y + \frac{1}{2} \left(b - \frac{a^2}{4} \right) y^2 + \frac{d}{2}x^2 + \dots \right\}, \quad (13)$$

from which one can obtain the matching to the coupling constants G_i according to

$$\begin{aligned} G_0 &= \mathcal{N} \left\{ 1 - \frac{a}{2} + \frac{1}{2} \left(b - \frac{a^2}{4} \right) \right\}, \\ G_1 &= \mathcal{N} \left\{ \frac{a}{2} - \left(b - \frac{a^2}{4} \right) \right\} \frac{M_\eta + 2M_{\pi^0}}{M_{\pi^0} Q_{\eta'}}, \\ G_2 &= \mathcal{N} \left(b - \frac{a^2}{4} \right) \frac{(M_\eta + 2M_{\pi^0})^2}{2M_{\pi^0}^2 Q_{\eta'}^2}, \quad G_3 = \mathcal{N} \frac{3d}{2Q_{\eta'}^2}. \end{aligned} \quad (14)$$

In the isospin limit, the charged-channel couplings H_i are related to the G_i via $H_i = -\sqrt{2}G_i$ (in the Condon-Shortley phase convention), which we will assume in the following.

The couplings C_i, D_i, E_i, F_i are obtained by matching to the effective range expansion of $\pi\pi$ and $\pi\eta$ scattering. The partial wave decomposition of the $\pi\pi$ scattering amplitude is conventionally written as [24]

$$T^I(s, t) = 32\pi \sum_{l=0}^{\infty} (2l+1) t_l^I(s) P_l(z), \quad (15)$$

where $t_l^I(s)$ is the partial wave amplitude of angular momentum l and isospin I , $P_l(z)$ are the Legendre polynomials, and $z = \cos\theta$ is the scattering angle in the center-of-mass system. Close to threshold of the pertinent channel, one can perform an expansion in the center-of-mass momentum $q_{ab}^2(s) = \lambda(s, M_a, M_b)/4s$ [with the standard Källén function $\lambda(a, b, c) = a^2 + b^2 + c^2 - 2(ab + ac + bc)$] according to

$$\text{Re } t_l^I(s) = q_{ab}^{2l} \left\{ a_l^I + b_l^I q_{ab}^2 + f_l^I q_{ab}^4 + \mathcal{O}(q_{ab}^6) \right\}. \quad (16)$$

As only $\pi\pi$ S-waves are considered in the following, we will use the slightly simplified notation a_0, a_2 for the S-wave scattering lengths of isospin 0 and 2, and similarly for the effective ranges b_i and shape parameters f_i .

We use a definition of the $\pi\eta$ threshold parameters strictly analogous to (15), (16), and denote the S- and P-wave scattering lengths and the S-wave effective range by \bar{a}_0, \bar{a}_1 , and \bar{b}_0 . These quantities are modified compared to the more conventional parameterization used in $\pi\eta$ scattering [25]; our $\pi\eta$ threshold parameters are related to the conventional ones $a_0^{\pi\eta}, a_1^{\pi\eta}, b_0^{\pi\eta}$ by

$$\bar{a}_i = \frac{M_\eta + M_\pi}{4} a_i^{\pi\eta}, \quad \bar{b}_0 = \frac{M_\eta + M_\pi}{4} \left(b_0^{\pi\eta} + \frac{a_0^{\pi\eta}}{2M_\pi M_\eta} \right). \quad (17)$$

We refrain from including the shape parameter of $\pi\eta$ -scattering; its contribution is expected to be tiny, and the threshold parameters of $\pi\eta$ -scattering are systematically smaller than those of $\pi\pi$ -scattering, c.f. Appendix B. Furthermore, even the leading threshold parameters of $\pi\eta$ -scattering are not easy to come by within a sensible error range, see [26] and Appendix B. However, the inclusion of higher orders in the modified non-relativistic framework is straightforward and can be easily performed, should the threshold parameters be obtained to greater accuracy.

We can fix the couplings of the non-relativistic Lagrangian by matching the amplitude of the effective theory to (16). The $\pi\pi$ and $\pi\eta$ Lagrangians generate the following tree amplitudes

$$\text{Re } T_i^{\pi\pi} = 2C_i + 8D_i q_{ab}^2 + 32F_i q_{ab}^4 + \dots, \quad (18)$$

$$\text{Re } T^{\eta a} = 2C_{\eta a} + 8D_{\eta a} q_{\eta a}^2 + E_{\eta a} \left(t - u + \frac{\Delta_{\eta a}^2}{s} \right) + \dots$$



Fig. 2.1. Non-relativistic two-loop graph involving the six-particle vertex. Double lines denote η' and η , the dashed line the π^0 .

The matching conditions can be simply read off: for $\pi\pi$ scattering we have [5, 8]

$$\begin{aligned} 2C_{00} &= \frac{N}{3}(a_0 + 2a_2)(1 - \xi), & 8D_{00} &= \frac{N}{3}(b_0 + 2b_2), \\ 2C_x &= \frac{N}{3}(a_2 - a_0)\left(1 + \frac{\xi}{3}\right), & 8D_x &= \frac{N}{3}(b_2 - b_0), \\ 2C_{+-} &= \frac{N}{6}(2a_0 + a_2)(1 + \xi), & 8D_{+-} &= \frac{N}{6}(2b_0 + b_2), \end{aligned} \quad (19)$$

and the matching conditions for the F_i are identical to those for the D_i with the replacements $b_i \rightarrow f_i/4$. Isospin breaking in the S-wave scattering lengths has been taken into account at leading order in chiral perturbation theory [27] in (19), $\xi = (M_\pi^2 - M_{\pi^0}^2)/M_\pi^2$, and $N = 32\pi$. For $\eta\pi$ scattering we find

$$\begin{aligned} 2C_{\eta 0} &= 2C_{\eta +} = N\bar{a}_0, & 8D_{\eta 0} &= 8D_{\eta +} = N\bar{b}_0, \\ 4E_{\eta 0} &= 4E_{\eta +} = 3N\bar{a}_1. \end{aligned} \quad (20)$$

2.3 6-particle vertices, inelastic channels

Six-particle interactions can be included in the modified non-relativistic framework by straightforward extension

$$\mathcal{L}_{\eta\pi\pi} = \frac{1}{4}F_0\eta^\dagger(\Phi_0^\dagger)^2\eta\Phi_0^2 + F_0'\eta^\dagger\Phi_+^\dagger\Phi_-^\dagger\eta\Phi_+\Phi_- + \dots, \quad (21)$$

where the ellipsis denotes terms with derivative couplings. To give a rough estimate of the contribution to the neutral channel, we perform a threshold expansion for the diagram in Fig. 2.1, which amounts to the application of the “classical” non-relativistic framework [28]. The real part is a constant (albeit divergent), which can be absorbed in a redefinition of the coupling G_0 and thus simply amounts to a change of the renormalization prescription. The imaginary part of the diagram is given by

$$\text{Im}\mathcal{A}_N^{\pi^0\pi^0\eta} = \frac{F_0G_0}{256\pi^2} \frac{M_{\pi^0}M_\eta^{1/2}}{(M_\eta + 2M_{\pi^0})^{3/2}} Q_{\eta'}^2 + \mathcal{O}(Q_{\eta'}^3). \quad (22)$$

We can give an estimate for F_0 by matching to chiral perturbation theory. At lowest order (assuming isospin symmetry), we find

$$F_0 = \frac{M_\pi^3}{36F_\pi^4} \left\{ \frac{5M_\pi}{M_\eta^2} - \frac{1}{M_\pi + M_\eta} \right\}, \quad (23)$$

where F_π is the pion decay constant. The imaginary part of the diagram can be mimicked by allowing G_0 to have a

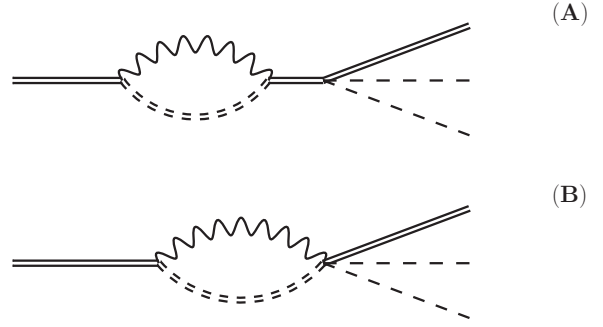


Fig. 2.2. Contributions of the inelastic $\rho^0\gamma$ channel. The double-dashed line denotes the ρ^0 , the wiggly line a photon; otherwise, the line style is as in Fig. 2.1.

small imaginary part. Numerically,

$$\frac{\text{Im } G_0}{\text{Re } G_0} \simeq 10^{-6}, \quad (24)$$

which is sufficiently small to assume the coupling constants of the non-relativistic Lagrangian to be real.

One may also wonder about effects of the finite width of the η' , or the coupling to inelastic channels other than $\eta\pi\pi$. One effect of the finite width is that the mass of the η' obtains an imaginary part; however, in view of $\Gamma_{\eta'}/M_{\eta'} \approx 2 \times 10^{-4}$, this is still negligible if we aim at an overall accuracy at the percent level at best. The largest decay channel of the η' other than $\eta\pi\pi$ is $\rho^0\gamma$ [29], which could contribute via the diagrams shown in Fig. 2.2. The rescattering vertex in diagram (B) is anomalous, but there is no $VV \rightarrow \eta\pi^0\pi^0$ vertex in the Wess–Zumino–Witten Lagrangian [30, 31], so we neglect this term. Diagram (A) leads to a complex wave-function renormalization factor Z , for which we find

$$\text{Im } Z_{\rho^0\gamma} = \frac{2M_{\eta'}^2 + M_\rho^2}{M_{\eta'}^2 - M_\rho^2} \frac{\Gamma_{\eta' \rightarrow \rho^0\gamma}}{M_{\eta'}} \approx 5 \times 10^{-4}. \quad (25)$$

This is therefore also an extremely small correction, which can furthermore be absorbed in an overall phase. We conclude that, for the purpose of this investigation, we can assume real coupling constants and neglect inelastic channels.

3 The decay amplitudes to two loops

We use the following decomposition of the amplitudes

$$\begin{aligned} \mathcal{M}_{\eta' \rightarrow \eta\pi^0\pi^0} &= \mathcal{M}_N^{\text{tree}} + \mathcal{M}_N^{1\text{-loop}} + \mathcal{M}_N^{2\text{-loop}} + \dots, \\ \mathcal{M}_{\eta' \rightarrow \eta\pi^+\pi^-} &= \mathcal{M}_C^{\text{tree}} + \mathcal{M}_C^{1\text{-loop}} + \mathcal{M}_C^{2\text{-loop}} + \dots, \end{aligned} \quad (26)$$

to underline that the tree amplitude of $\mathcal{L}_{\eta' \rightarrow \eta\pi\pi}$ is modified by final state interactions of one, two, etc. loops.

3.1 Tree amplitudes

The tree amplitudes are given by

$$\begin{aligned}\mathcal{M}_N^{\text{tree}}(s_1, s_2, s_3) &= \sum_{i=0}^2 G_i X_3^i + G_3 (X_1 - X_2)^2, \\ \mathcal{M}_C^{\text{tree}}(s_1, s_2, s_3) &= \sum_{i=0}^2 H_i X_3^i + H_3 (X_1 - X_2)^2,\end{aligned}\quad (27)$$

where $X_k = p_k^0 - M_\eta$, $k = 1, 2, 3$.

3.2 One-loop amplitudes

For the one-loop amplitudes we find

$$\begin{aligned}\mathcal{M}_N^{1\text{-loop}}(s_1, s_2, s_3) &= \mathcal{B}_{N1}(s_3)J_{+-}(s_3) + \mathcal{B}_{N2}(s_3)J_{00}(s_3) \\ &\quad + \{\mathcal{B}_{N3}(s_1, s_2, s_3)J_{\eta 0}(s_1) + (s_1 \leftrightarrow s_2)\}, \\ \mathcal{M}_C^{1\text{-loop}}(s_1, s_2, s_3) &= \mathcal{B}_{C1}(s_3)J_{+-}(s_3) + \mathcal{B}_{C2}(s_3)J_{00}(s_3) \\ &\quad + \{\mathcal{B}_{C3}(s_1, s_2, s_3)J_{\eta+}(s_1) + (s_1 \leftrightarrow s_2)\},\end{aligned}\quad (28)$$

with the one-loop function

$$J_{ab}(s_k) = \frac{iq_{ab}(s_k)}{8\pi\sqrt{s_k}}, \quad (29)$$

and the polynomials

$$\begin{aligned}\mathcal{B}_{N1}(s_3) &= 2C_x(s_3) \left\{ \sum_{i=0}^2 H_i X_3^i + H_3 \frac{4\mathbf{Q}_3^2}{3s_3} q_{+-}^2(s_3) \right\}, \\ \mathcal{B}_{N2}(s_3) &= C_{00}(s_3) \left\{ \sum_{i=0}^2 G_i X_3^i + G_3 \frac{4\mathbf{Q}_3^2}{3s_3} q_{00}^2(s_3) \right\}, \\ \mathcal{B}_{N3}(s_1, s_2, s_3) &= 2C_{\eta 0}(s_1) \left\{ G_0 + G_1 Z_{1,+}^{\eta 0} \right. \\ &\quad + G_2 \left[(Z_{1,+}^{\eta 0})^2 + \frac{\mathbf{Q}_1^2}{3s_1} q_{\eta 0}^2(s_1) \right] \\ &\quad + G_3 \left[(Z_{1,-}^{\eta 0} - X_1)^2 + \frac{\mathbf{Q}_1^2}{3s_1} q_{\eta 0}^2(s_1) \right] \\ &\quad \left. - E_{\eta 0} \frac{q_{\eta 0}^2(s_1)}{3M_{\eta'}} \left[s_3 - s_2 + \frac{\Delta_{\eta 0}}{s_1} (M_{\eta'}^2 - M_{\pi^0}^2) \right] \right\} \\ &\quad \times \left\{ G_1 + 2G_2 Z_{1,+}^{\eta 0} + 2G_3 (X_1 - Z_{1,-}^{\eta 0}) \right\},\end{aligned}\quad (30)$$

for the neutral channel, and

$$\begin{aligned}\mathcal{B}_{C1}(s_3) &= 2C_{+-}(s_3) \left\{ \sum_{i=0}^2 H_i X_3^i + H_3 \frac{4\mathbf{Q}_3^2}{3s_3} q_{+-}^2(s_3) \right\}, \\ \mathcal{B}_{C2}(s_3) &= C_x(s_3) \left\{ \sum_{i=0}^2 G_i X_3^i + G_3 \frac{4\mathbf{Q}_3^2}{3s_3} q_{00}^2(s_3) \right\}, \\ \mathcal{B}_{C3}(s_1, s_2, s_3) &= 2C_{\eta+}(s_1) \left\{ H_0 + H_1 Z_{1,+}^{\eta+} \right.\end{aligned}$$

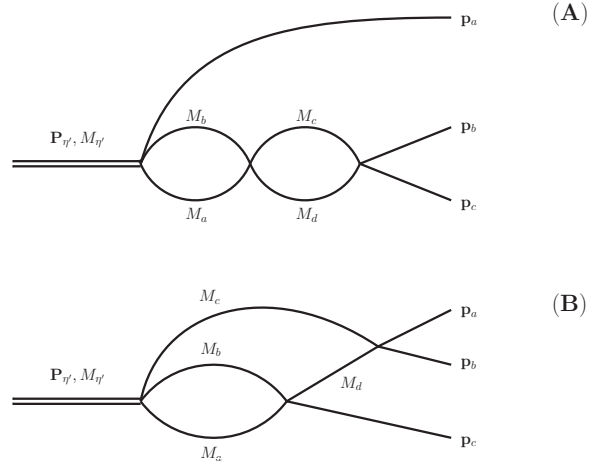


Fig. 3.1. The two distinct topologies appearing at two loops. The first one (A) is a simple product of one-loop functions, the second one (B) yields a more complicated analytic behavior. Here, the double line denotes the η' , while single lines stand generically for any of the particles in the final state η , π^\pm , and π^0 .

$$\begin{aligned}&+ H_2 \left[(Z_{1,+}^{\eta+})^2 + \frac{\mathbf{Q}_1^2}{3s_1} q_{\eta+}^2(s_1) \right] \\ &+ H_3 \left[(Z_{1,-}^{\eta+} - X_1)^2 + \frac{\mathbf{Q}_1^2}{3s_1} q_{\eta+}^2(s_1) \right] \Big\} \\ &- E_{\eta+} \frac{q_{\eta+}^2(s_1)}{3M_{\eta'}} \left[s_3 - s_2 + \frac{\Delta_{\eta+}}{s_1} (M_{\eta'}^2 - M_\pi^2) \right] \\ &\times \left\{ H_1 + 2H_2 Z_{1,+}^{\eta+} + 2H_3 (X_1 - Z_{1,-}^{\eta+}) \right\},\end{aligned}\quad (31)$$

for the charged channel. The following abbreviations have been used:

$$\begin{aligned}Q_a^0 &= p_b^0 + p_c^0 \text{ (+cycl.)}, \quad \mathbf{Q}_a^2 = \frac{\lambda(M_{\eta'}^2, M_a^2, s_a)}{4M_{\eta'}^2}, \\ Z_{k,\pm}^{ab} &= \frac{Q_k^0}{2} \left(1 \pm \frac{\Delta_{ab}}{s_k} \right) - M_a,\end{aligned}\quad (32)$$

$$C_{bc}(s_a) = C_{bc} + 4D_{bc}q_{bc}^2(s_a) + 16F_{bc}q_{bc}^4(s_a), \quad q_x = q_{+-}.$$

Note in particular that there are no higher orders in the $\pi\eta$ mass difference omitted in the P-wave of $\pi\eta$ scattering; with our Lagrangian definition of the P-wave operators, the formulae above are exact.

3.3 Two-loop amplitudes

The two-loop amplitudes contain diagrams of two distinct topologies, see Fig. 3.1. We find the following

$$\begin{aligned}\mathcal{M}_N^{2\text{-loop}}(s_1, s_2, s_3) &= C_{00}(s_3)\mathcal{B}_{N2}(s_3)J_{00}^2(s_3) \\ &\quad + \left[C_{00}(s_3)\mathcal{B}_{N1}(s_3) + 2C_x(s_3)\mathcal{B}_{C2}(s_3) \right] J_{00}(s_3)J_{+-}(s_3) \\ &\quad + 2C_x(s_3)\mathcal{B}_{C1}(s_3)J_{+-}^2(s_3) \\ &\quad + \left\{ 2C_{\eta 0}(s_1)\mathcal{B}_{N3}(s_1, s_2, s_3)J_{\eta 0}^2(s_1) \right.\end{aligned}$$

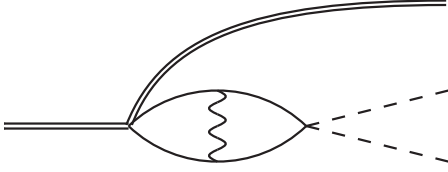


Fig. 3.2. Leading contribution to radiative corrections in $\eta' \rightarrow \eta\pi^0\pi^0$. The wiggly line denotes the exchange of a Coulomb photon between two charged pions (single full lines).

$$\begin{aligned}
& + 2G_0 C_{00} C_{\eta 0} F_0(M_{\pi^0}, M_{\pi^0}, M_{\eta}, M_{\pi^0}, s_1) \\
& + 4H_0 C_x C_{\eta 0} F_0(M_{\pi}, M_{\pi}, M_{\eta}, M_{\pi^0}, s_1) \\
& + 4G_0 C_{\eta 0}^2 F_0(M_{\eta}, M_{\pi^0}, M_{\pi^0}, M_{\eta}, s_1) + (s_1 \leftrightarrow s_2) \Big\} \\
& + 4G_0 C_{\eta 0} C_{00} F_{\eta}(M_{\eta}, M_{\pi^0}, M_{\pi^0}, M_{\pi^0}, s_3) \\
& + 8H_0 C_{\eta+} C_x F_{\eta}(M_{\eta}, M_{\pi}, M_{\pi}, M_{\pi}, s_3) \quad (33)
\end{aligned}$$

in the neutral channel, and

$$\begin{aligned}
\mathcal{M}_C^{2\text{-loop}}(s_1, s_2, s_3) = & 2C_{+-}(s_3) \mathcal{B}_{C1}(s_3) J_{+-}^2(s_3) \\
& + \left[C_x(s_3) \mathcal{B}_{N1}(s_3) + 2C_{+-}(s_3) \mathcal{B}_{C2}(s_3) \right] J_{00}(s_3) J_{+-}(s_3) \\
& + C_x(s_3) \mathcal{B}_{N2}(s_3) J_{00}^2(s_3) \\
& + \left\{ 2C_{\eta+}(s_1) \mathcal{B}_{C3}(s_1, s_2, s_3) J_{\eta+}^2(s_1) \right. \\
& + 4H_0 C_{+-} C_{\eta+} F_+(M_{\pi}, M_{\pi}, M_{\eta}, M_{\pi}, s_1) \\
& + 2G_0 C_x C_{\eta+} F_+(M_{\pi^0}, M_{\pi^0}, M_{\eta}, M_{\pi}, s_1) \\
& + 4H_0 C_{\eta+}^2 F_+(M_{\eta}, M_{\pi}, M_{\pi}, M_{\eta}, s_1) + (s_1 \leftrightarrow s_2) \Big\} \\
& + 8H_0 C_{\eta+} C_{+-} F_{\eta}(M_{\eta}, M_{\pi}, M_{\pi}, M_{\pi}, s_3) \\
& + 4G_0 C_{\eta 0} C_x F_{\eta}(M_{\eta}, M_{\pi^0}, M_{\pi^0}, M_{\pi^0}, s_3) \quad (34)
\end{aligned}$$

in the charged channel. The analytic form of the genuine two-loop function $F_k(M_a, M_b, M_c, M_d, s_k)$ can be found in Appendix A. The representation above is valid to $\mathcal{O}(a_{\pi\pi}^2 \epsilon^6, a_{\pi\pi} a_{\pi\eta} \epsilon^2, a_{\pi\eta}^2 \epsilon^2)$. Due to the smallness of the $\pi\eta$ rescattering effects, this is well justified.

3.4 Radiative corrections

In [6], radiative corrections to $K \rightarrow 3\pi$ decays have been discussed in the framework of non-relativistic effective field theory. The results obtained there for the decay channels $K_L \rightarrow 3\pi^0$ and $K_L \rightarrow \pi^+\pi^-\pi^0$ can be adapted immediately to $\eta' \rightarrow \eta\pi\pi$ decays, so we only quote the final formulae and refer to [6] for the derivation.

In the neutral decay $\eta' \rightarrow \eta\pi^0\pi^0$, no “external” radiative corrections exist. The leading electromagnetic contributions (of $\mathcal{O}(a_{\pi\pi} \log \epsilon)$) are due to virtual-photon exchange inside a charged-pion loop, see Fig. 3.2. These become important very close to threshold, as they modify the analytic structure near the cusp by adding a logarithmic singularity to the square-root-like behavior. The diagram in Fig. 3.2 can be taken into account by the following re-

placement of the charged-pion one-loop function:

$$\begin{aligned}
J_{+-}(s_3) & \rightarrow J_{+-}(s_3) + \bar{J}_C(s_3), \\
\bar{J}_C(s_3) & = -\frac{\alpha}{32\pi} \log \left(-\frac{4q_{+-}^2(s_3)}{M_{\pi}^2} \right). \quad (35)
\end{aligned}$$

As $\eta' \rightarrow \eta\pi^+\pi^-$ only serves as the “auxiliary channel” in the cusp analysis, only radiative corrections of $\mathcal{O}(e^2 a^0)$ are considered, hence we neglect photon exchange inside loops. The external photon corrections, comprising virtual-photon exchange as well as real-photon radiation up to a maximal photon energy E^* , can be subsumed in the correction factor $\Omega_C(s_3, E^*)$ that multiplies the decay spectrum, which is given in the soft-photon approximation by

$$\left. \frac{d\Gamma}{ds_3} \right|_{E_{\gamma} < E^*} = \Omega_C(s_3, E^*) \frac{d\Gamma^{\text{int}}}{ds_3}, \quad (36)$$

$$\Omega_C(s_3, E^*) = 1 + \frac{\alpha}{\pi} \left\{ \frac{\pi^2(1 + \sigma^2)}{2\sigma} + \frac{8}{3} \sigma^2 \left[\log \frac{2E^*}{M_{\pi}} - \frac{1}{3} \right] \right\},$$

where $\sigma = \sqrt{1 - 4M_{\pi}^2/s_3}$. To the accuracy considered here, $d\Gamma^{\text{int}}/ds_3$ is the $\eta' \rightarrow \eta\pi^+\pi^-$ decay spectrum without photon corrections. See [6] for the more elaborate result without the soft-photon approximation.

4 Prediction of the cusp

In the previous section, we have given the representation of the $\eta' \rightarrow \eta\pi\pi$ decay amplitudes to two-loop order in terms of a set of coupling constants G_i , H_i , as well as $\pi\pi$ and $\pi\eta$ threshold parameters. In order to extract the $\pi\pi$ scattering length combination $a_0 - a_2$, one would have to fit the latter together with the couplings G_i (and possibly even H_i if one wishes to relax the assumption on isospin conservation in the polynomial terms) to experimental data. Here we wish to *predict* the cusp in $\eta' \rightarrow \eta\pi^0\pi^0$. For this purpose, we first have to fix parameters.

The $\pi\pi$ scattering lengths and effective ranges are set to the theoretical values $a_0 = 0.220 \pm 0.005$, $a_2 = -0.0444 \pm 0.0010$, $b_0 = (0.276 \pm 0.006) \times M_{\pi}^{-2}$, $b_2 = (-0.0803 \pm 0.0012) \times M_{\pi}^{-2}$ [32], and the shape parameters f_0, f_2 to 0. There is no experimental information on the $\pi\eta$ threshold parameters, and as discussed in Appendix B, theoretical constraints from chiral perturbation theory are not very restrictive. We will therefore discuss the uncertainties induced by this lack of knowledge by varying these parameters in the ranges $\bar{a}_0 = (0 \dots +16) \times 10^{-3}$, $\bar{b}_0 = (0 \dots +10) \times 10^{-3} M_{\pi}^{-2}$, $\bar{a}_1 = (-1 \dots +1) \times 10^{-3} M_{\pi}^{-2}$. We find however (in agreement with [33]) that the effects of the P-wave \bar{a}_1 are absolutely negligible (about two orders of magnitude smaller than the changes induced by the variation in the $\pi\eta$ S-wave shown in the following), and therefore set $\bar{a}_1 = 0$ in the sequel.

There is no very precise information on the $\eta' \rightarrow \eta\pi\pi$ Dalitz plot parameters. We will use the central values (without errors) of the most recent determinations done

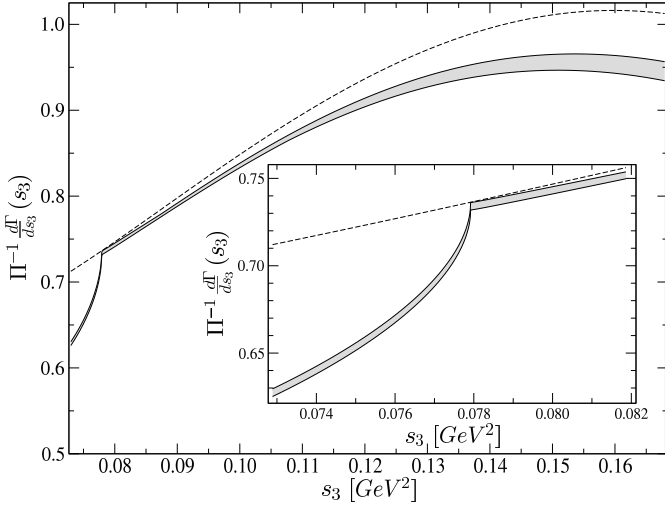


Fig. 4.1. The decay rate $d\Gamma/ds_3$ divided by phase space. The Dalitz plot parameters have been matched to the tree-level amplitude. The dashed line is the tree result, the gray band shows the full result under variation of the $\pi\eta$ threshold parameters. The insert focuses on the cusp region around the $\pi^+\pi^-$ threshold.

by the VES collaboration for the charged channel [34], which, adjusting the normalization to the neutral decay, read $a = -0.133$, $b = -0.116$, $d = -0.094$. We have checked using rather different older data on the neutral channel ($a = -0.116$, $b = d = 0$ [35]) that, while the overall Dalitz plot distribution of course looks very different, all statements about the cusp behavior hold in exactly the same way. We only discuss normalized decay spectra, setting $\mathcal{N} = 1$.

The decay spectrum $d\Gamma/ds_3$ for $\eta' \rightarrow \eta\pi^0\pi^0$ is calculated by

$$\frac{d\Gamma}{ds_3} = \frac{1}{512\pi^3 M_{\eta'}^3} \int_{s_1^-(s_3)}^{s_1^+(s_3)} ds_1 |\mathcal{M}_N(s_1, s_3)|^2, \quad (37)$$

$$s_1^\pm(s_3) = M_\eta^2 + M_{\pi^0}^2 + \frac{1}{2} \left\{ M_{\eta'}^2 - M_\eta^2 - s_3 \right. \\ \left. \pm \frac{1}{s_3} \lambda^{1/2}(M_{\eta'}^2, M_\eta^2, s_3) \lambda^{1/2}(s_3, M_{\pi^0}^2, M_{\pi^0}^2) \right\},$$

which we normalize by the phase space factor

$$\Pi(s_3) = \frac{s_1^+(s_3) - s_1^-(s_3)}{512\pi^3 M_{\eta'}^3}. \quad (38)$$

In Fig. 4.1 we display the normalized decay spectrum $\Pi^{-1}(s_3)d\Gamma/ds_3$ for $\eta' \rightarrow \eta\pi^0\pi^0$, with the coupling constants G_i , H_i matched to the VES Dalitz plot parameters directly according to (14). The cusp effect is prominently visible below the charged-pion threshold and amounts to a reduction of the decay spectrum up to around 10%. Furthermore, the final-state interaction reduces the spectrum for large s_3 by about 5%, largely due to $\pi\pi$ rescattering. The effects generated by varying $\pi\eta$ threshold parameters (as seen by the gray band in Fig. 4.1) are moderate, but particularly small in the cusp region. We remark that the

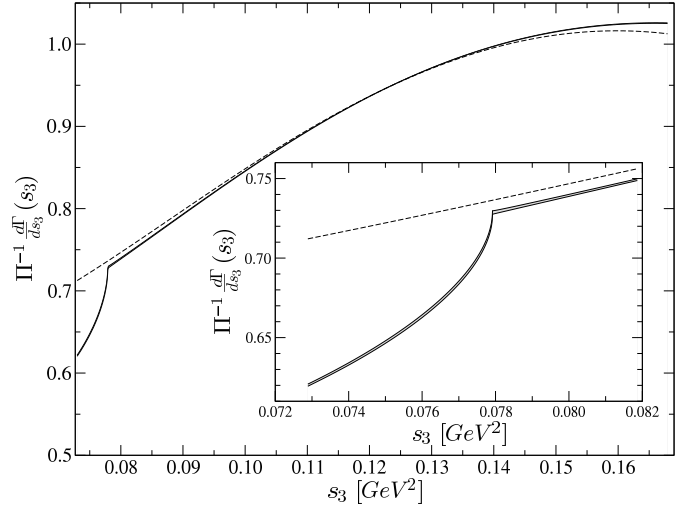


Fig. 4.2. The decay rate $d\Gamma/ds_3$ divided by phase space. The Dalitz plot parameters have been matched to the full amplitude. We show tree (dashed) and full result (solid), the latter again for varying $\pi\eta$ threshold parameters. Effects of these parameters are observed to be significantly reduced compared to Fig. 4.1. The insert magnifies the $\pi^+\pi^-$ threshold region.

sign of the cusp is fixed by (approximate) isospin symmetry, $H_i = -\sqrt{2}G_i$.

It is obvious from Fig. 4.1 that the amplitude does not reproduce the experimental Dalitz plot parameters any more – they are renormalized by the final-state interactions. We therefore re-adjust the tree-level couplings such that the *full* amplitude squared (10) yields the VES parameters. The renormalized tree-level parameters, according to (14), e.g. correspond to $\mathcal{N}_{\text{ren}} = 1.015$ (1.021), $a_{\text{ren}} = -0.168$ (−0.181), $b_{\text{ren}} = -0.108$ (−0.106), $d_{\text{ren}} = -0.099$ (−0.097), for $\bar{a}_0 = 0.016$, $\bar{b}_0 = 0.010 M_\pi^{-2}$ ($\bar{a}_0 = 0$, $\bar{b}_0 = 0$). The decay spectra resulting from this procedure are shown in Fig. 4.2. We see that the full result follows the tree-level spectrum closely except for small deviations close to the kinematic limits, and the prominent cusp below the $\pi^+\pi^-$ threshold. The uncertainty band due to $\pi\eta$ scattering has shrunk to a very narrow line: the effects of the third-particle rescattering can be absorbed to a large extent in a redefinition of the polynomial part.

Integrating the spectrum in the region $4M_{\pi^0}^2 \leq s_3 \leq 4M_\pi^2$, we find that the cusp reduces the number of events in that region with respect to the tree distribution (or no $\pi\pi$ rescattering) by more than 8%, compared to about 13% in $K^+ \rightarrow \pi^0\pi^0\pi^+$ (see e.g. [36]), or less than 2% in $\eta \rightarrow 3\pi^0$ [11].

In Fig. 4.3 we zoom in further into the cusp region to investigate the expected two-loop cusp above threshold. We plot the decay spectrum, with the tree spectrum subtracted, shifted to 0 at threshold,

$$R(s_3) = \Pi^{-1}(s_3) \left[\frac{d\Gamma_{\text{full}}}{ds_3} - \frac{d\Gamma_{\text{tree}}}{ds_3} \right] \\ - \Pi^{-1}(4M_\pi^2) \left[\frac{d\Gamma_{\text{full}}}{ds_3} - \frac{d\Gamma_{\text{tree}}}{ds_3} \right]_{s_3=4M_\pi^2}. \quad (39)$$

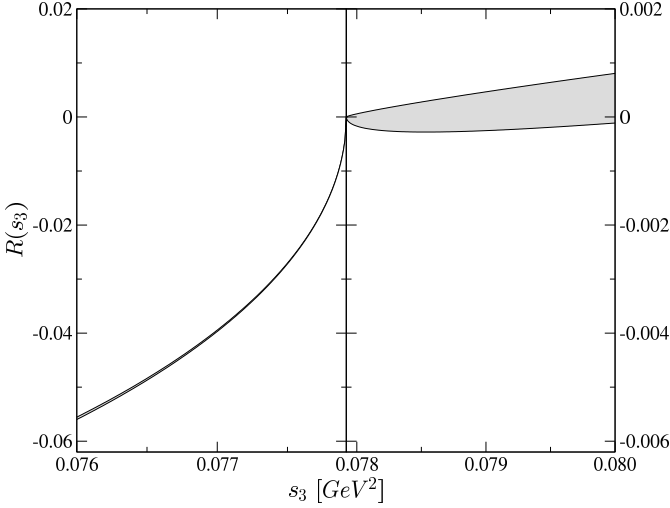


Fig. 4.3. Difference between full and tree decay rate $d\Gamma/ds_3$ in the cusp region, divided by the phase space, and shifted to 0 at $s_3 = 4M_\pi^2$. Note that the scale above the cusp has been increased by a factor of 10.

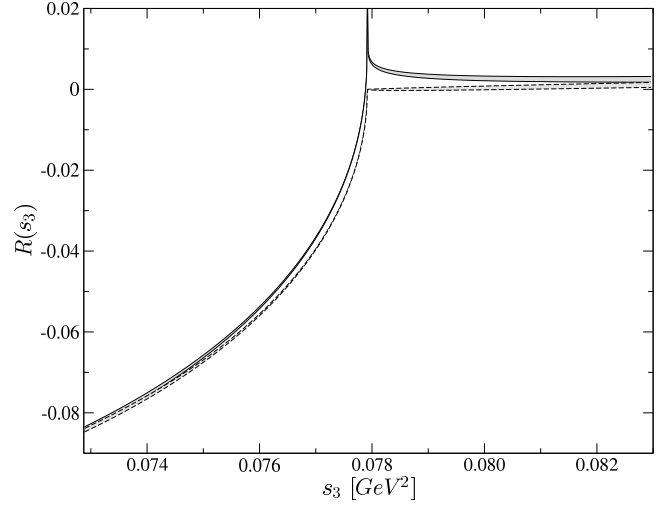


Fig. 4.4. Difference between full and tree decay rate $d\Gamma/ds_3$ in the cusp region, divided by the phase space. The dashed band is without, the full band with radiative corrections. The latter displays the logarithmic singularity at threshold, compare (35).

We increase the scale above threshold by a factor of 10. Obviously the two-loop cusp (above threshold) is highly suppressed compared to the one-loop cusp (below threshold). One would expect the two-loop cusp effect to be smaller than the one generated by one-loop diagrams, as it is suppressed by another power in $\pi\pi$ or $\pi\eta$ threshold parameters; however, a suppression by more than two orders of magnitude may seem surprising at first. The explanation for this observation can be found resorting to the *threshold theorem* [1, 5, 6]: in the direct vicinity of the $\pi^+\pi^-$ threshold, one can parameterize the amplitude (up to three loops, in the absence of photons) as

$$\mathcal{M}_N = \alpha_0 + i(\alpha_1 + \alpha'_1 q_{+-}(s_3)) + (\alpha_2 - \alpha'_2 q_{+-}(s_3)) + i(\alpha_3 + \alpha'_3 q_{+-}(s_3)) + \mathcal{O}(a^4), \quad (40)$$

where the real parameters α_i , α'_i are of $\mathcal{O}(a^i)$. This leads to

$$|\mathcal{M}_N|^2 = \text{reg.} - 2(\alpha_0(\alpha'_1 + \alpha'_3) + \alpha_2\alpha'_1 + \alpha_1\alpha'_2) \times \sqrt{-q_{+-}^2(s_3)} + \mathcal{O}(a^5) \quad (41)$$

below threshold, where “reg.” denotes polynomial (non-singular) terms in the vicinity of $s_3 = 4M_\pi^2$, and

$$|\mathcal{M}_N|^2 = \text{reg.} - 2(\alpha_0\alpha'_2 - \alpha_1\alpha'_1)q_{+-}(s_3) + \mathcal{O}(a^4) \quad (42)$$

above threshold. The threshold theorem states that the coefficients α'_i are proportional to \mathcal{M}_C in the appropriate kinematics,

$$\mathcal{M}_C(s_1 = s_2, s_3 = 4M_\pi^2) \propto \alpha'_1 + i\alpha'_2 + \alpha'_3 + \mathcal{O}(a^3), \quad (43)$$

where the factor of proportionality includes the $\pi\pi$ charge-

exchange scattering length, while obviously

$$\mathcal{M}_N(s_1 = s_2, s_3 = 4M_\pi^2) = \alpha_0 + i\alpha_1 + \alpha_2 + \mathcal{O}(a^3). \quad (44)$$

In the isospin limit $\alpha_i \propto -\sqrt{2}\alpha'_{i+1}$ and, according to (42), the two-loop effects on the cusp would exactly cancel. Numerically, we find with our set of parameters

$$\begin{aligned} \mathcal{M}_C(s_1 = s_2, s_3 = 4M_\pi^2) &= -1.22 \text{ (tree)} - 0.076i \text{ (1-loop)} \\ &\quad + 0.0046 \text{ (2-loop)}, \\ \mathcal{M}_N(s_1 = s_2, s_3 = 4M_\pi^2) &= 0.86 \text{ (tree)} + 0.050i \text{ (1-loop)} \\ &\quad - 0.0039 \text{ (2-loop)}, \end{aligned} \quad (45)$$

which leads to a suppression of the two-loop cusp by about a factor of 250. Incidentally, (41) also allows to estimate the effect of three-loop (or $\mathcal{O}(a^3)$) contributions to the cusp, which do *not* vanish in the isospin limit. We find that $\mathcal{O}(a^3)$ terms ought to reduce the leading $\mathcal{O}(a)$ cusp by about 0.5%. Therefore we conclude that, unlike in $K^+ \rightarrow \pi^0\pi^0\pi^+$ decays, where two-loop contributions are an essential ingredient to the proper theoretical description of the amplitude in the threshold region, the cusp in $\eta' \rightarrow \eta\pi^0\pi^0$ is entirely dominated by the leading $\mathcal{O}(a)$ rescattering effects.

Finally, we briefly comment on the effect of the radiative corrections discussed in Sect. 3.4. Figure 4.4 shows the cusp region similarly to Fig. 4.3, with and without the replacement (35). While the logarithmic singularity at threshold is visible, the effect becomes very small away from $s_3 = 4M_\pi^2$. These corrections clearly only matter in experimental analyses with very high resolution and statistics.

5 Summary and conclusion

In this article, we have generalized the formalism of non-relativistic effective field theory to describe the analytic structure, and in particular the cusp effect, in $\eta' \rightarrow \eta\pi\pi$ decays. We have shown how to construct an effective Lagrangian that reproduces the next-to-leading threshold parameters (effective range, P-wave scattering length) in $\pi\eta$ scattering, and derived the decay amplitudes up to two loops, including $\mathcal{O}(\epsilon^4)$, $\mathcal{O}(a\epsilon^5)$, $\mathcal{O}(a_{\pi\pi}^2\epsilon^6, a_{\pi\pi}a_{\pi\eta}\epsilon^2, a_{\pi\eta}^2\epsilon^2)$. These amplitudes are the central result of our investigation, and ought to be employed in future precision studies of the $\eta' \rightarrow \eta\pi\pi$ Dalitz plot.

Invoking theoretical information on the coupling constants involved, we have also *predicted* the size of the cusp effect, and shown that it reduces the decay spectrum below the charged-pion threshold by more than 8%. This is a much more sizeable effect than e.g. in $\eta \rightarrow 3\pi^0$ decays. Approximate isospin symmetry dictates that the cusp of $\mathcal{O}(a^2)$ above threshold is strongly suppressed, and three-loop effects can be estimated to yield a correction below 1%. Therefore the threshold singularity in $\eta' \rightarrow \eta\pi^0\pi^0$ is determined to very high precision by the leading $\mathcal{O}(a)$ rescattering effect. Experimental verifications of these predictions at various laboratories [16–23] are eagerly awaited.

Acknowledgements. We would like to thank Akaki Rusetsky for useful discussions, and Martin Hoferichter for comments on the manuscript. Partial financial support by the Helmholtz Association through funds provided to the virtual institute “Spin and strong QCD” (VH-VI-231), by the European Community-Research Infrastructure Integrating Activity “Study of Strongly Interacting Matter” (acronym Hadron-Physics2, Grant Agreement n. 227431) under the Seventh Framework Programme of the EU, and by DFG (SFB/TR 16, “Subnuclear Structure of Matter”) is gratefully acknowledged.

A The two-loop function

The analytic representation of the two-loop formula is given as [8]

$$F_k(M_a, M_b, M_c, M_d, s_k) = \bar{\mathcal{N}}(2Af_1 + Bf_0) + \mathcal{O}(\epsilon^4), \quad (46)$$

with

$$\bar{\mathcal{N}} = \frac{1}{256\pi^3\sqrt{s_k}} \frac{\lambda^{1/2}(s_0, M_a^2, M_b^2)}{s_0\sqrt{\Delta^2 - \frac{(1+\delta)^2}{4}\mathbf{Q}_k^2}},$$

$$f_0 = 4(v_1 + v_2 - \bar{v}_2 + h),$$

$$f_1 = \frac{4}{3}(y_1(v_1 - 1) + y_2(v_2 - 1) - \bar{y}_2(\bar{v}_2 - 1) + h),$$

$$h = \frac{1}{2} \log \left(\frac{1 + \mathbf{Q}_k^2/s_k}{1 + \bar{\mathbf{Q}}_k^2/\bar{s}_k} \right), \quad \bar{\mathbf{Q}}_k^2 = \mathbf{Q}_k^2(\bar{s}_k),$$

$$v_i = \sqrt{-y_i} \arctan \frac{1}{\sqrt{-y_i}}, \quad i = 1, 2;$$

$$\begin{aligned} \bar{v}_2 &= \sqrt{-\bar{y}_2} \arctan \frac{1}{\sqrt{-\bar{y}_2}}, \quad \bar{y}_2 = y_2(\bar{s}_k), \\ \bar{s}_k &= (M_c + M_d)^2, \\ y_{1,2} &= \frac{-B \mp \sqrt{B^2 - 4AC}}{2A}, \quad A = -\frac{\mathbf{Q}_k^2}{s_k}(M_c^2 + \Delta^2), \\ B &= q_{cd}^2(s_k) - \Delta^2 + \frac{\mathbf{Q}_k^2}{s_k}M_c^2, \quad C = -q_{cd}^2(s_k), \\ s_0 &= M_{\eta'}^2 + M_c^2 - 2M_{\eta'} \left(M_c^2 + \frac{\mathbf{Q}_k^2(1+\delta)^2}{4} \right)^{1/2}, \\ \Delta^2 &= \frac{\lambda(M_{\eta'}^2, M_c^2, (M_a + M_b)^2)}{4M_{\eta'}^2}, \quad \delta = \frac{M_c^2 - M_d^2}{s_k}. \end{aligned} \quad (47)$$

B $\pi\eta$ threshold parameters

$\pi\eta$ scattering has been calculated up to $\mathcal{O}(p^4)$ in chiral perturbation theory (ChPT) in [25]. We use the form quoted in [37] for the expansion near threshold. The scattering lengths $a_0^{\pi\eta}$ and $a_1^{\pi\eta}$ are discussed extensively in [26].

The S-wave $\pi\eta$ scattering length to $\mathcal{O}(p^4)$ is given by²

$$\begin{aligned} \bar{a}_0 &= \frac{M_\pi^2}{96\pi F_\pi^2} \left\{ 1 + \frac{96}{F_\pi^2} \left[\left(L_1^r + L_2^r + \frac{L_3}{2} - L_4^r - \frac{L_5^r}{6} + L_6^r \right. \right. \right. \\ &\quad \left. \left. - L_7 \right) M_\eta^2 + \left(L_7 + \frac{L_8}{2} \right) M_\pi^2 \right] - \frac{1}{16\pi^2 F_\pi^2} \left[3M_\pi^2 \log \frac{M_\pi}{\mu} \right. \\ &\quad \left. + (15M_\eta^2 + M_\pi^2) \log \frac{M_K}{\mu} + \left(\frac{4}{3}M_\eta^2 + M_\pi^2 \right) \log \frac{M_\eta}{\mu} \right. \\ &\quad \left. \left. - \frac{4M_\pi^4}{3(M_\eta^2 - M_\pi^2)} \log \frac{M_\pi}{M_\eta} + A_+ + A_- - \frac{25M_\eta^2 + 7M_\pi^2}{3} \right] \right\}, \\ A_\pm &= (3M_\eta \pm M_\pi)^2 \frac{\sqrt{2M_\eta(M_\eta \mp M_\pi)}}{M_\eta \pm M_\pi} \\ &\quad \times \arctan \left(\frac{M_\eta \pm M_\pi}{\sqrt{2M_\eta(M_\eta \mp M_\pi)}} \right), \end{aligned} \quad (48)$$

where we have made use of the Gell-Mann–Okubo relation $4M_K^2 = 3M_\eta^2 + M_\pi^2$ in the $\mathcal{O}(p^4)$ corrections. \bar{a}_0 can be related to the $I = 2$ $\pi\pi$ scattering length

$$\begin{aligned} a_0^2 &= -\frac{M_\pi^2}{16\pi F_\pi^2} \left\{ 1 - \frac{32M_\pi^2}{F_\pi^2} \left[L_1^r + L_2^r + \frac{L_3}{2} - L_4^r - \frac{L_5^r}{2} \right. \right. \\ &\quad \left. \left. + L_6^r + \frac{L_8}{2} \right] + \frac{M_\pi^2}{16\pi^2 F_\pi^2} \left[3 \log \frac{M_\pi}{\mu} + \frac{1}{9} \log \frac{M_\eta}{\mu} - \frac{4}{9} \right] \right\}, \end{aligned} \quad (49)$$

as well as $\Delta_F = F_K/F_\pi - 1$ and $\Delta_{\text{GMO}} = (4M_K^2 - 3M_\eta^2 - M_\pi^2)/(M_\eta^2 - M_\pi^2)$ [38] in the form of the low-energy theo-

² All $\pi\eta$ threshold parameters are given in the isospin limit. Note that isospin breaking in $\pi\eta$ at tree-level only affects the scattering length at $\mathcal{O}((m_u - m_d)^2)$ and is therefore negligible; there are no electromagnetic effects at that order.

rem

$$\begin{aligned} \bar{a}_0 = & \frac{M_\pi^2}{96\pi F_\pi^2} \left\{ 1 + \frac{48\pi F_\pi^2 M_\eta^2}{M_\pi^4} \Delta a_0^2 + \frac{8}{3} \frac{3M_\eta^2 + M_\pi^2}{M_\eta^2 - M_\pi^2} \Delta_F \right. \\ & + \frac{4}{3} \Delta_{\text{GMO}} + \frac{1}{16\pi^2 F_\pi^2} \left[\frac{9M_\eta^4 - 6M_\eta^2 M_\pi^2 + M_\pi^4}{3(M_\eta^2 - M_\pi^2)} \log \frac{M_\pi}{M_\eta} \right. \\ & + 2 \frac{3M_\eta^4 - 10M_\eta^2 M_\pi^2 - M_\pi^4}{M_\eta^2 - M_\pi^2} \log \frac{M_\pi}{M_K} - A_+ - A_- \\ & \left. \left. + 7 \left(M_\eta^2 + \frac{M_\pi^2}{3} \right) \right] \right\}, \end{aligned} \quad (50)$$

where $\Delta a_0^2 = a_0^2 + M_\pi^2/(16\pi F_\pi^2)$. We find the (modified) $\pi\eta$ effective range \bar{b}_0 and P-wave scattering length \bar{a}_1 at $\mathcal{O}(p^4)$

$$\begin{aligned} \bar{b}_0 = & \frac{1}{\pi F_\pi^4} \left\{ \left(L_1^r + L_2^r + \frac{L_3}{2} - \frac{L_4^r}{2} \right) (M_\eta^2 + M_\pi^2) \right. \\ & + \left(L_2^r + \frac{L_3}{3} \right) M_\pi M_\eta \left. \right\} + \frac{1}{512\pi^3 F_\pi^4} \left\{ \frac{4}{3} M_\pi^2 \log \frac{M_\pi}{M_K} \right. \\ & + \frac{2M_\pi^4(3M_\eta^2 - 2M_\eta M_\pi + 3M_\pi^2)}{9(M_\eta - M_\pi)^3(M_\eta + M_\pi)} \log \frac{M_\pi}{M_\eta} - \frac{\tilde{A}_+}{6} \\ & - 7 \left(M_\eta^2 + \frac{6}{7} M_\pi M_\eta + M_\pi^2 \right) \log \frac{M_K}{\mu} - \frac{(M_\eta^2 + M_\pi^2)\tilde{A}_-}{6(M_\eta - M_\pi)^2} \\ & + \left[135M_\eta^6 - 108M_\eta^5 M_\pi + 107M_\eta^4 M_\pi^2 - 214M_\eta^3 M_\pi^3 \right. \\ & \left. + 177M_\eta^2 M_\pi^4 - 2M_\eta M_\pi^5 + M_\pi^6 \right] (54M_\eta^2(M_\eta - M_\pi)^2)^{-1} \left. \right\}, \\ \bar{a}_1 = & -\frac{1}{3\pi F_\pi^4} \left\{ \left(L_1^r + \frac{L_3}{6} - \frac{L_4^r}{2} \right) (M_\eta^2 + M_\pi^2) \right. \\ & - \left(L_2^r + \frac{L_3}{3} \right) M_\eta M_\pi \left. \right\} + \frac{1}{4608\pi^3 F_\pi^4} \left\{ 4M_\pi^2 \log \frac{M_\pi}{\mu} \right. \\ & - \frac{2M_\pi^4(M_\eta + M_\pi)}{3(M_\eta - M_\pi)^3} \log \frac{M_\pi}{M_\eta} + \frac{M_\eta M_\pi \tilde{A}_-}{(M_\eta - M_\pi)^2} \\ & - \left(3M_\eta^2 - 18M_\pi M_\eta + 7M_\pi^2 \right) \log \frac{M_K}{\mu} \\ & - \left[27M_\eta^6 + 108M_\eta^5 M_\pi - 215M_\eta^4 M_\pi^2 + 214M_\eta^3 M_\pi^3 \right. \\ & \left. - 39M_\eta^2 M_\pi^4 + 2M_\eta M_\pi^5 - M_\pi^6 \right] (18M_\eta^2(M_\eta - M_\pi)^2)^{-1} \left. \right\}, \\ \tilde{A}_\pm = & \frac{12M_\eta^4 \pm 3M_\eta^3 M_\pi - 15M_\eta M_\pi^2 (M_\eta \pm M_\pi) - M_\pi^4}{2M_\eta^2(3M_\eta \pm M_\pi)(M_\eta \mp M_\pi)} A_\pm. \end{aligned} \quad (51)$$

As the $\pi\pi$ scattering amplitude in SU(3) only depends on the linear combination $2L_1^r + L_3$ [37], it is obvious that one cannot formulate low-energy theorems for \bar{b}_0 and \bar{a}_1 in terms of $\pi\pi$ threshold parameters (or πK scattering lengths [39]). We therefore refrain from recasting these results in alternative forms.

We use two different sets of $\mathcal{O}(p^4)$ low-energy constants for numerical evaluation [40, 41]. A major difficulty consists in estimating the combined errors, as the various uncertainties for the low-energy constants are strongly

| | CA | Ref. [40] | Ref. [41] | LET |
|--------------------------|-----------------|-----------------|------------------|-----------------|
| $10^3 \bar{a}_0$ | 7.6 | 15.7 ± 23.9 | 9.8 ± 15.8 | -0.2 ± 7.7 |
| $10^3 M_\pi^2 \bar{b}_0$ | 0 | 9.9 ± 22.9 | 0.4 ± 18.8 | — |
| $10^3 M_\pi^2 \bar{a}_1$ | 0 | 0.9 ± 3.7 | -0.8 ± 2.3 | — |
| | $(\pi\pi)_{00}$ | | $(\pi\pi)_x$ | $(\pi\pi)_{+-}$ |
| $10^3 a_0$ | | 40.9 ± 1.7 | -90.0 ± 1.7 | 70.2 ± 1.7 |
| $10^3 M_\pi^2 b_0$ | | 38.5 ± 2.0 | -118.8 ± 2.0 | 78.6 ± 2.0 |
| $10^3 M_\pi^2 a_1$ | | — | — | 19.0 ± 0.3 |

Table B.1. Numerical results for the $\pi\eta$ threshold parameters. The first column “CA” refers to the $\mathcal{O}(p^2)$ values, the second and third column show the $\mathcal{O}(p^4)$ results, evaluated with the low-energy constants taken from [40, 41]. Errors are obtained naively by adding individual uncertainties in quadrature. The lower three columns show the $\pi\pi$ threshold parameters for the physical channels elastic $\pi^0\pi^0$ scattering $(\pi\pi)_{00}$, charge exchange $(\pi\pi)_x$, and elastic $\pi^+\pi^-$ $(\pi\pi)_{+-}$. For details, see text.

correlated. The errors quoted in Table B.1 are obtained by naive error propagation, neglecting any correlations; we consider the uncertainties thus obtained significantly overestimated. In the case of \bar{a}_0 , we also use the low-energy theorem (50), with $\Delta a_0^2 = 0.0012 \pm 0.0010$ [32], $\Delta_{\text{GMO}} = 0.196$, and $\Delta_F = 0.193 \pm 0.006$ [29]. Table B.1 shows the results for \bar{a}_0 , \bar{b}_0 , \bar{a}_1 thus obtained; in the cases of \bar{a}_0 and \bar{a}_1 , these are consistent with the findings in [26]. The conclusion is that chiral symmetry does not make very precise predictions for the $\pi\eta$ threshold parameters. The next-to-leading order corrections for \bar{a}_0 can be as large as the current-algebra value, the magnitude of the effective range is very badly constrained, and not even the sign is fixed for \bar{a}_1 . For numerical evaluation in the main text, we decide to vary the $\pi\eta$ threshold parameters in the ranges $\bar{a}_0 = (0 \dots +16) \times 10^{-3}$, $\bar{b}_0 = (0 \dots +10) \times 10^{-3} M_\pi^{-2}$, $\bar{a}_1 = (-1 \dots +1) \times 10^{-3} M_\pi^{-2}$. We consider these reasonable, although not the most conservative limits possible. They comprise the values given in [25] and most of the parameter ranges discussed in [26].

To put these numbers into perspective, Table B.1 also shows the $\pi\pi$ threshold parameters [32] for the different physical channels (corrected for tree-level isospin breaking in the S-wave scattering lengths [27]), in the same units. The errors are approximate only and, in case of the S-waves, propagated from the dominant $I = 0$ threshold parameters. The comparison demonstrates that, even within a large uncertainty range, $\pi\eta$ scattering in general is much weaker than $\pi\pi$ scattering and should therefore have far less influence on the decay properties of $\eta' \rightarrow \eta\pi\pi$ via final-state interactions. We furthermore remark that a simple unitarization model [42] (that reproduces the $a_0(980)$ resonance within reasonable accuracy) indicates that the $\pi\eta$ phase stays below 5° in the range up to $\sqrt{s} \leq M_{\eta'} - M_{\pi^0} \approx 823$ MeV, therefore the influence of the $a_0(980)$ resonance is not yet severe and the effective range expansion still applicable.

References

1. N. Cabibbo, Phys. Rev. Lett. **93** (2004) 121801 [arXiv:hep-ph/0405001].
2. N. Cabibbo and G. Isidori, JHEP **0503** (2005) 021 [arXiv:hep-ph/0502130].
3. J. R. Batley *et al.* [NA48/2 Collaboration], Phys. Lett. B **633** (2006) 173 [arXiv:hep-ex/0511056].
4. E. Gámiz, J. Prades and I. Scimemi, Eur. Phys. J. C **50** (2007) 405 [arXiv:hep-ph/0602023].
5. G. Colangelo, J. Gasser, B. Kubis and A. Rusetsky, Phys. Lett. B **638** (2006) 187 [arXiv:hep-ph/0604084].
6. M. Bissegger, A. Fuhrer, J. Gasser, B. Kubis and A. Rusetsky, Nucl. Phys. B **806** (2009) 178 [arXiv:0807.0515 [hep-ph]].
7. U.-G. Meißner, G. Müller and S. Steininger, Phys. Lett. B **406** (1997) 154 [Erratum-ibid. B **407** (1997) 454] [arXiv:hep-ph/9704377].
8. M. Bissegger, A. Fuhrer, J. Gasser, B. Kubis and A. Rusetsky, Phys. Lett. B **659** (2008) 576 [arXiv:0710.4456 [hep-ph]].
9. E. Abouzaida *et al.* [KTeV Collaboration], Phys. Rev. D **78** (2008) 032009 [arXiv:0806.3535 [hep-ex]].
10. C. Ditsche, B. Kubis and U.-G. Meißner, Eur. Phys. J. C **60** (2009) 83 [arXiv:0812.0344 [hep-ph]].
11. C.-O. Gullström, A. Kupść and A. Rusetsky, Phys. Rev. C **79** (2009) 028201 [arXiv:0812.2371 [hep-ph]].
12. C. Adolph *et al.* [WASA-at-COSY Collaboration], arXiv:0811.2763 [nucl-ex].
13. M. Unverzagt *et al.* [Crystal-Ball-at-MAMI, TAPS, and A2 Collaborations], Eur. Phys. J. A **39** (2009) 169 [arXiv:0812.3324 [hep-ex]].
14. S. Prakhov *et al.* [Crystal-Ball-at-MAMI and A2 Collaborations], Phys. Rev. C **79** (2009) 035204 [arXiv:0812.1999 [hep-ex]].
15. R. Nißler, PhD thesis, University of Bonn (2008) [http://hss.ulb.uni-bonn.de/diss_online/math_nat_fak/2008/nissler_robin].
16. Project C.5 of the SFB/TR 16, “Subnuclear Structure of Matter”, U. Wiedner, R. Beck *et al.*.
17. A. Starostin, in *Proc. 2nd Int. Workshop on Eta Meson Physics, Peñíscola, Spain, 2007*, edited by M. Jacewicz and B. Hoistad, arXiv:0710.1809 [nucl-ex].
18. P. Achenbach, arXiv:0802.2870 [nucl-ex].
19. H. H. Adam *et al.* [WASA-at-COSY Collaboration], arXiv:nucl-ex/0411038.
20. B. R. Jany and D. Duniec [WASA-at-COSY Collaboration], *Proc. 11th Int. Conf. on Meson–Nucleon Physics and the Structure of the Nucleon (MENU 2007), Jülich*.
21. KLOE-2, Letter of Intent [http://www.lnf.infn.it/lnf-admin/direzione/roadmap/LoIKLOE.pdf].
22. C. Bloise, AIP Conf. Proc. **950** (2007) 192.
23. H. B. Li, arXiv:0902.3032 [hep-ex].
24. B. Ananthanarayan, G. Colangelo, J. Gasser and H. Leutwyler, Phys. Rept. **353** (2001) 207 [arXiv:hep-ph/0005297].
25. V. Bernard, N. Kaiser and U.-G. Meißner, Phys. Rev. D **44** (1991) 3698.
26. M. Kolesár and J. Novotný, Eur. Phys. J. C **56** (2008) 231 [arXiv:0802.1289 [hep-ph]].
27. M. Knecht and R. Urech, Nucl. Phys. B **519** (1998) 329 [arXiv:hep-ph/9709348].
28. J. Gasser, V. E. Lyubovitskij and A. Rusetsky, Phys. Rept. **456** (2008) 167 [arXiv:0711.3522 [hep-ph]].
29. C. Amsler *et al.* [Particle Data Group], Phys. Lett. B **667** (2008) 1.
30. J. Wess and B. Zumino, Phys. Lett. B **37** (1971) 95.
31. E. Witten, Nucl. Phys. B **223** (1983) 422.
32. G. Colangelo, J. Gasser and H. Leutwyler, Nucl. Phys. B **603** (2001) 125 [arXiv:hep-ph/0103088].
33. B. Borasoy and R. Nißler, Eur. Phys. J. A **26** (2005) 383 [arXiv:hep-ph/0510384].
34. V. Dorofeev *et al.*, Phys. Lett. B **651** (2007) 22 [arXiv:hep-ph/0607044].
35. D. Alde *et al.* [Serpukhov-Brussels-Los Alamos-Annecy (LAPP) Collaboration], Phys. Lett. B **177** (1986) 115 [Sov. J. Nucl. Phys. **45** (1987 YAFIA,45,117-122.1987) 75.1987 YAFIA,45,117].
36. D. Madigozhin, *Pion scattering lengths from the cusp effect analysis*, talk given at: FlaviAnet Kaon Workshop, June 12–14, 2008, Anacapri, Italy.
37. A. Gómez Nicola and J. R. Peláez, Phys. Rev. D **65** (2002) 054009 [arXiv:hep-ph/0109056].
38. J. Gasser and H. Leutwyler, Nucl. Phys. B **250** (1985) 465.
39. B. Kubis and U.-G. Meißner, Phys. Lett. B **529** (2002) 69 [arXiv:hep-ph/0112154].
40. J. Bijnens, G. Ecker and J. Gasser, arXiv:hep-ph/9411232.
41. G. Amoros, J. Bijnens and P. Talavera, Nucl. Phys. B **585** (2000) 293 [Erratum-ibid. B **598** (2001) 665] [arXiv:hep-ph/0003258].
42. J. A. Oller, E. Oset and J. R. Peláez, Phys. Rev. D **59** (1999) 074001 [Erratum-ibid. D **60** (1999) 099906, Erratum-ibid. D **75** (2007) 099903] [arXiv:hep-ph/9804209].